Eur. J. Mech., B/Fluids, **16,** n° 2, 211-226, 1997

Spectral analysis of the turbulent structure in the momentumless wake of a propeller-driven body

T. FAURE and G. ROBERT *

ABSTRACT. – Wind tunnel measurements of the velocity spectra behind a propeller-driven model with a momentumless wake are described. Immediately behind the body the spectra display marked peaks associated with the propeller rotation. These peaks become less marked downstream, the periodic effect becoming negligible beyond five body diameters behind the model, and they are concentrated in a limited zone directly affected by the rotor. The wide-band part of the radial velocity spectrum indicates a maximum near the normalised frequency $\beta \sim 4$, possibly associated with large turbulent structures near the wake boundary. In the far-wake the spectra tend to become self-similar.

1. Introduction

The investigation of the turbulent structure in the momentumless wake of a propeller-driven body is of interest because of its direct applicability to naval and aeronautical devices. In this configuration, the drag of the body is cancelled by a thrust, so that the momentum integral, which expresses the difference between thrust and drag, is equal to zero. It is of interest to investigate the effect of this initial condition on the development of the turbulent flow although, particularly with respect to spectral analysis, there are relatively few published studies.

Axisymmetric momentumless wakes were first investigated by Schooley and Stewart (1963) in a stratified fluid at a Reynolds number based on the diameter of the body $\mathrm{Re}_D = 9900$; they observed slower entrainment in the vertical than in the horizontal direction but did not give data for the velocity field inside the wake. The benchmark experimentation for a self-propelled body is that of Naudascher (1965): a circular disk with a coaxial jet at its centre was placed in a wind tunnel at a Reynolds number based on the diameter of the disk $\mathrm{Re}_D = 5.5 \times 10^4$. He pointed out that, whereas the self-similar profiles for simple jets and wakes require only a single amplitude and width scaling, those for the momentumless wake depend on a number of additional normalising scales. The measurement of some of the terms of the turbulent kinetic energy balance led to the conclusion that the production term was very small in comparison with the convection term.

* Laboratoire de Mécanique des Fluides et d'Acoustique, UMR CNRS 5509, École Centrale de Lyon, 69131 Écully Cedex, France.

0997-7546/97/02/$ 7.00/

A comparison between a propeller-driven slender body and a peripheral-jet model was carried out by Swanson *et al.* (1974), Chieng *et al.* (1974) and Schetz and Jakubowski (1975). The Reynolds number was $\mathrm{Re}_D = 6 \times 10^5$ and they observed that the wake development of a blunt body driven by a central jet to yield a zero momentum wake was quite different from the wake of a body driven by a peripheral jet.

Another noteworthy experiment is the investigation in the momentumless wake of an axisymmetric jet-propelled body, by Higuchi and Kubota (1990). They tested the influence of injection and showed that the relaxation zone depended on the turbulence in the initial wake.

The near region of the wake of a momentumless, propeller-driven body was compared with the wake generated by a body with a rotating hub without blades by Hyun and Patel (1991). The Reynolds number was $\mathrm{Re}_D = 1.53 \times 10^5$. They processed the velocity measurements in phase with the propeller rotation and observed structures induced by each blade in a region that extended to two diameters downstream of the body.

Two-dimensional self-propelled wakes have been studied experimentally by Cimbala and Park (1990) and Park and Cimbala (1991) where a momentumless configuration was obtained using jet injection at Reynolds number $\mathrm{Re}_D = 5400$. These authors found self-similarity of the axial and transverse turbulence intensities. The behaviour of turbulence was quite different from that of plane wakes with drag or jets bur rather similar to grid turbulence. The type of injection (central or peripheral jet) was found to be an important parameter for the rate of decay of mean velocity and for spreading, however it had no influence on the axial turbulence intensity. The first of these two studies is the only one where spectral analysis is carried out in a momentumless wake, a two-dimensional, jet-driven case. While a Kármán vortex shedding frequency and its harmonics are present for a wake with drag, there are no such identifiable peaks when self-propulsion is established. Noteworthy in the radial spectra is the maximum that occurs at the edge of the wake, which indicates that there exists a quasi-periodic vertical motion caused by some sort of large turbulent structure near the wake boundary.

Some spectral data are available for wakes with drag, where there is vortex shedding; we mention in a non-exhaustive list the experiments of Cimbala *et al.* (1988), Jones *et al.* (1988) and Cimbala and Krein (1990) for two-dimensional circular cylinder wakes. The experiment of Peterson and Hama (1978) performed in the axisymmetric wake of a slender body of revolution at $\mathrm{Re}_D = 3600$ leads to the conclusion that the far-wake is the region in which non-linear interactions appear to predominate. Finally, self-preservation of spectra was shown in the far-wake of a two-dimensional cylinder by Wygnanski *et al.* (1986).

The objective of the present investigation is to provide spectral data for the axisymmetric momentumless wake of a propeller-driven body. An experiment is performed in a wind tunnel and a complete characterisation from the near to the far region is obtained. The analysis of the power spectral density functions will lead to the observation, in the near region of the wake, of spectral peaks associated with the propeller rotation and the periodic blade passage. The study of the turbulent structures will be conducted in the outer part of the wake. Then, the evolution of the wide-band part of the

spectra to self-similar behaviour will be shown for the far-wake. The similarity of the spectra in this region to homogeneous isotropic turbulence will suggest that turbulence in the momentumless far-wake may be treated as isotropic. The difficulties of measuring the dissipation function will be discussed.

2. Experimental arrangements and signal processing

The wake is generated by an axisymmetric, streamlined body mounted in the working section of a wind tunnel (500 mm $\times$ 500 mm, 6 m long). The experimental freestream velocity can vary from 5 m/s to 80 m/s with a uniformity of $\pm$ 2% and a maximum turbulence intensity of 0.7%. The model diameter D is 8 cm and the length is 50 cm. It has an elliptical nose, a cylindrical middle section and a conical stern. The propulsion system consists of a three-blade marine type propeller with a diameter of 4 cm. The inside of the body is hollow and contains the motor (15,000 rpm maximum speed) which drives the propeller. An electronic system is available to control the rotation speed. A support having a symmetrical NACA 66_1 012 profile with a chord of 10 cm and a maximum width of 1.2 cm was chosen to minimise aerodynamic perturbations around the body. Electrical wires for power supply and speed regulation are carried through this support. Provision was made for adjustment of the model with the freestream. Once this adjustment was made, the angle between the wake axis and the tunnel axis was found to be less than 0.3°. In the text, all the axial distances are measured from the trailing edge of the body and scaled on its diameter D.

For a self-propelled body, the drag generated by the model equals the thrust created by the propulsion system. To bring about this state a momentum balance was established for the model. To this effect, we have two parameters which can vary, the freestream velocity and the propeller rotation speed. The propeller rotation was fixed at its maximum value and the freestream velocity was varied to make the drag equal to the thrust (*Fig.* 1). Self-propulsion was established with a freestream velocity $U_e = 11.6$ m/s. The corresponding Reynolds number based on the diameter of the body was $\mathrm{Re}_D = 5.8 \times 10^4$.

The flow is three-dimensional and turbulent; it is therefore necessary to use a directional probe that can measure both the mean and the fluctuating parts of the velocity. An automated triple hot-film anemometry system was developed that gives all three components of instantaneous total velocity. The probe is a Dantec 55R91 type, with the active lengths of the three sensors included into a sphere of diameter $d = 1.2$ mm. Each sensor is a nickel film deposited on a quartz cylinder, 70 μm in diameter. The three film supports are orthogonal and inserted into a sphere of 3 mm diameter. This dimension corresponds to the Taylor scale of the structures encountered in the flow. The smallest Kolmogorov microscale is $\eta = 0.4$ mm, which may be compared with the measurement volume according to the criterion $d \leq 3 - 4\eta$ given by Wyngaard and Pao (1971). Calibration of each sensor is performed in the unperturbed freestream. Periodic verification is carried out during the acquisition procedure: the probe is placed in the freestream from time to time and a calibration point obtained for each film. As part of the signal processing, such points are used to update the calibration curve. This procedure

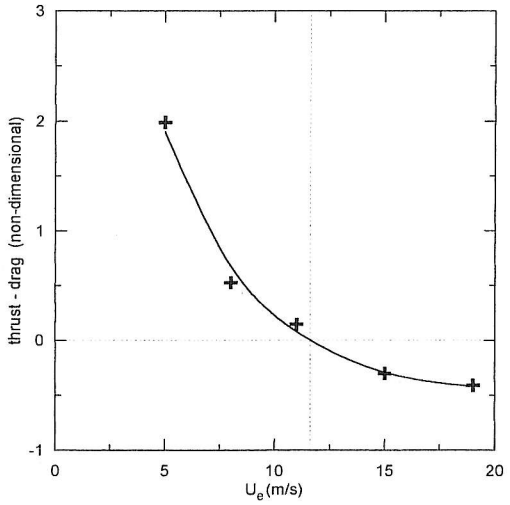

Fig. 1. – Variation of the thrust-drag balance (non-dimensional) with the freestream velocity.

avoids the influence of any change in the ambient temperature. The films are operated as constant temperature anemometers at an overheat ratio of 0.8. Output voltages from the anemometers are passed through offset and gain circuits. The signal is then analog filtered with a low-pass filter at a cut-off frequency that is half the sampling frequency, before being digitised with a 12 bit A-D converter. The data are stored on the hard disk of a 80386 PC computer for later processing. The various error sources throughout the acquisition procedure are carefully identified (Faure, 1995). Finally, the maximum global measurement errors are estimated to be 1.7% for mean velocity, 1.4% for second moments and 2.7% for triple moments.

When measuring spectra, an accurate bandwidth for low frequencies and a wide range of frequencies are needed. Thus, in order to obtain a single spectrum, two data acquisitions are carried out:

– a low-frequency-acquisition with a sampling frequency $f_{\mathrm{samp}} = 7.5$ kHz and an acquisition time $t_{\mathrm{samp}} = 20$ s;

– a high-frequency-acquisition with a sampling frequency $f_{\mathrm{samp}} = 50$ kHz and an acquisition time $t_{\mathrm{samp}} = 3$ s.

In each case 150,000 samples are taken for every point of measurement. Once these two spectra are measured, they are connected at a frequency of 1 kHz below which there is 95% of the turbulent energy. The mean-squared value of the error e is given according to Bendat and Piersol (1986) by:

$$e \approx \frac{1}{\sqrt{2\Delta f T}}$$

where T denotes the integration time and Δf is the frequency resolution. In the present study, an error of 8.3% is found.

3. The near-wake and the intermediate region

The radial evolution of the power spectral density function for the axial velocity fluctuations $E_{x,x}$ is plotted for different radial positions in Figure 2. The axial location in the momentumless wake is $x/D = 1$ and the radial coordinate is normalised with the radius of the model R. All the profiles for $0.25 \leq r/R \leq 0.75$ show peaks at the frequencies $f_0 = 250$ Hz and $3f_0$, that are associated respectively with the propeller rotation rate and the blade passing frequency. Harmonics of the first, $2f_0$ and $4f_0$, are also present but they are smaller in magnitude. Note that there is no peak in the inner part of the wake ($r/R \leq 0.25$). This region is associated with the wake of the propeller hub, and there is no influence of the periodic motion. Furthermore, for $r/R > 0.75$, there is again no peak in the spectrum. As a consequence, the rotation is restricted to a wake core while the outer region remains without swirl influence. The confinement of the rotation shows a behaviour quite different from isolated swirling motions. This effect may be typical of a momentumless rotor-driven wake. In fact, in any momentumless wake, there is a peripheral velocity deficit in the mean axial velocity profile, resulting from the drag effects. So, the isolation of the swirling motion in a central region may be due to these confinement effects. It is also noticeable in this figure that the wide-band part is decreasing from the centre to the freestream. A rapid change in the slope of spectra, in the high-frequency domain, appears from $r/R \sim 0.5$. This corresponds to a greater rate of decrease for the small turbulent structures. For the low frequencies, which contain most of the turbulent energy, the level falls rapidly at the wake boundary where $r/R = 0.625$. This means that turbulence is lower at the edge and in the freestream than in the core of the wake, and this transition is strongly marked. Therefore the turbulence intensity would be a good criterion to indicate the wake boundary.

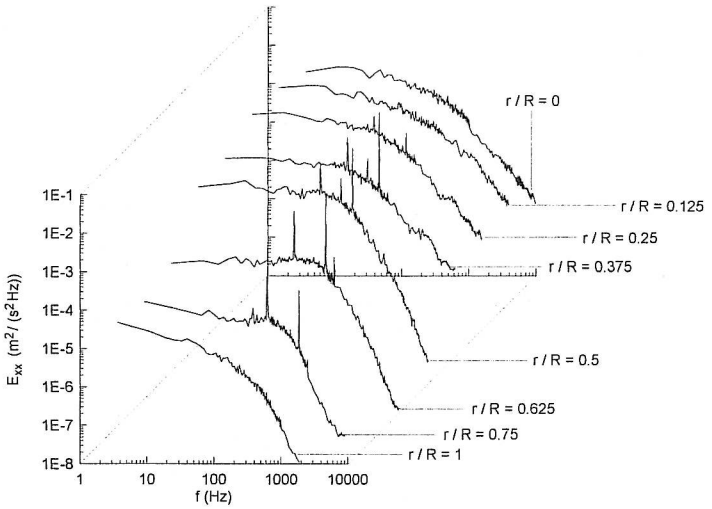

Fig. 2. – Radial evolution of the power spectral density function of the axial velocity fluctuations for the axial location $x/D = 1$.

The radius of the wake r^* is defined as the radial location where the axial turbulence intensity has fallen to half of its maximum value. An important position in the flow is the edge of the wake, corresponding to $r/R = 0.625$ in Figure 2 or $r/r^* = 1$. If we look at the axial evolution of spectral density functions for this particular location (*Fig.* 3), it is interesting to see that the wide-band level of turbulent structures is increasing with the axial distance, and that the spectral peaks for frequencies f_0 and $3f_0$ are always present. The harmonics $2f_0$ and $4f_0$ remain in the spectrum up to $x/D = 1$. For greater distances (*Fig.* 4) the wide-band part of the spectra is characterised by a decreasing level. The spectral peaks vanish, when $x/D > 2$ for $3f_0$ and when $x/D > 5$ for f_0. Downstream of this location, the wake is not marked by any forced periodic motion. This evolution may be compared with the axial evolution of the maximum turbulence intensity (*Fig.* 5). For $x/D < 2$ this level remains approximately constant and it starts to decrease from this distance. In the near wake, the turbulent energy is concentrated in spectral peaks due to the periodic motion, and transferred to the turbulence (the peaks feed the wide-band); the turbulence levels remains constant (*Fig.* 5) while the wide-band spectrum is increasing. In the intermediate region, for $2 < x/D < 10$, the spectral peaks vanish, and there is no more transfer from the periodic motion to turbulence. Consequently, the maximum turbulence intensity is decreasing, as is shown in Figure 5. For further axial locations, the change in the slope leads to another turbulent behaviour in the far-wake which will be discussed below.

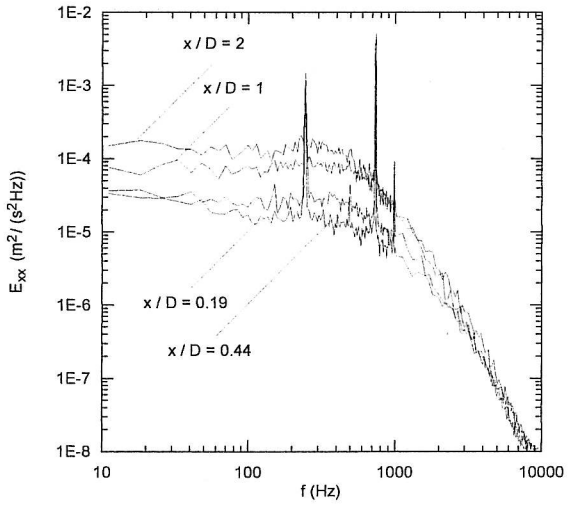

Fig. 3. – Axial evolution for $x/D \leq 2$ of the power spectral density function of the axial velocity fluctuations for the radial location $r/r^* = 1$.

The axial evolution of the peak level for the characteristic frequencies f_0 and $3f_0$ is presented for axial, radial and azimuthal power spectral density functions, at the boundary of the wake, in Figures 6-8. In every plot, the peak value is compared with the wide-band spectral level around the corresponding frequency, and of course when there is no more peak in the spectrum the two curves are identical. Generally, note that peak levels for the axial and radial spectra are quite close, while the levels for the

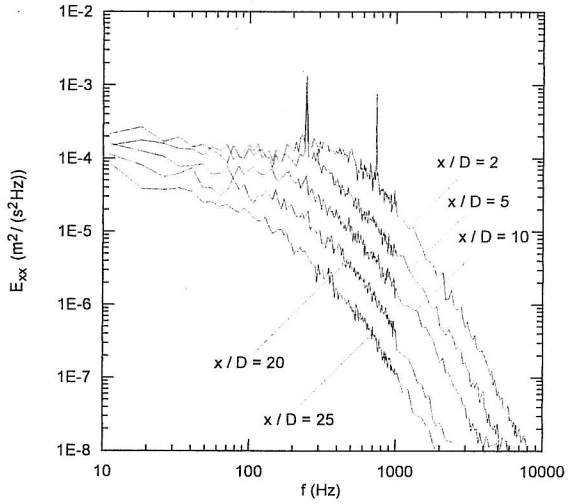

Fig. 4. – Axial evolution for $x/D \geq 2$ of the power spectral density function of the axial velocity fluctuations for the radial location $r/r^* = 1$.

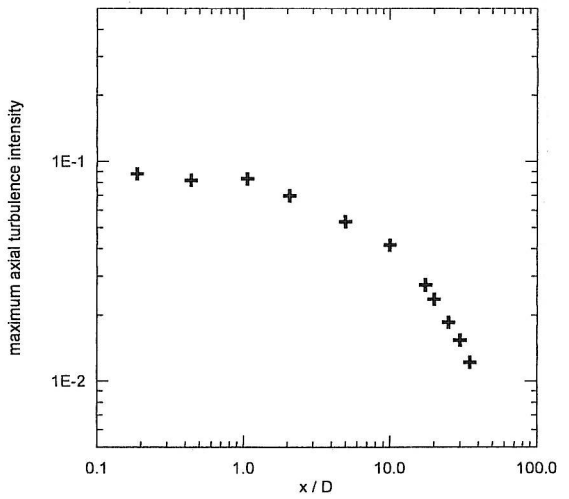

Fig. 5. – Axial evolution of the maximum axial turbulence intensity.

azimuthal spectra are somewhat different, even if the general evolution is the same. For the spectra of the axial velocity, in the region $x/D \leq 1$, the blade passing frequency $3f_0$ takes the highest level, which means that the coherent structures induced by the blade contain more energy than the global rotation motion. It is worth noticing that in this zone, the peak levels are constant and the wide-band level is increasing; there is creation of turbulent energy. For $x/D = 2$, there is a change in the dominating frequency, the level at frequency f_0 becomes higher that the level at frequency $3f_0$. Then, the spectral peak at $3f_0$ vanishes rapidly around $x/D = 5$ whereas the peak at f_0 remains up to $x/D = 10$. Throughout this region, there is a transfer of energy between the peak and the wide-band spectrum. Regarding the azimuthal spectrum the change in the dominant

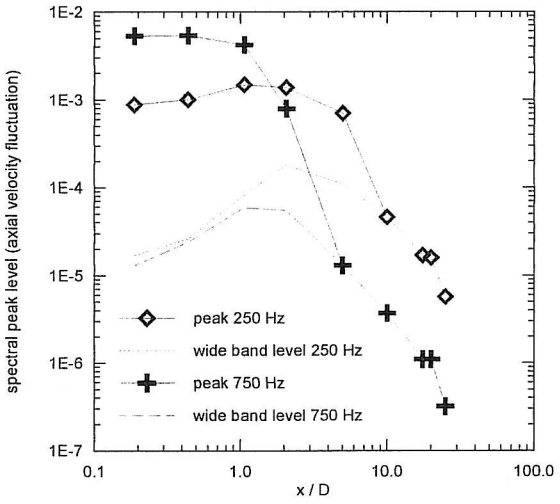

Fig. 6. – Axial evolution of the spectral peaks for frequencies $f_0 = 250$ Hz and $3f_0 = 750$ Hz (axial velocity fluctuations).

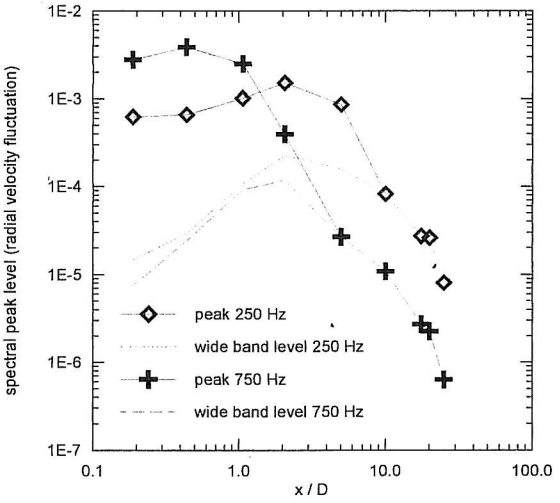

Fig. 7. – Axial evolution of the spectral peaks for frequencies $f_0 = 250$ Hz and $3f_0 = 750$ Hz (radial velocity fluctuations).

peak occurs further downstream, for $x/D > 2$. For $x/D \geq 10$, all spectral peaks have vanished and turbulence levels fall as a result of dissipation.

If we turn our mind to the power spectral density functions of the radial velocity fluctuations, at the radial location where $r/r^* = 1$, the spectra display a marked maximum at relatively low frequencies. In order to enhance this phenomenon and to remove the effects of the periodic motion, the signal is filtered for $f < 50$ Hz and spectral peaks at frequencies f_0 and $3f_0$ are removed when they are present. Then all the curves are

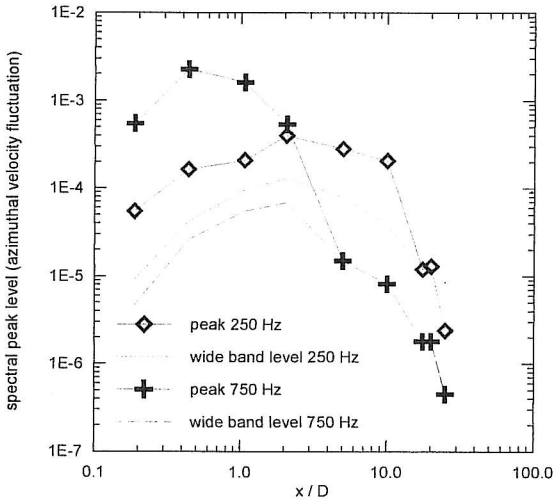

Fig. 8. – Axial evolution of the spectral peaks for frequencies $f_0 = 250$ Hz and $3f_0 = 750$ Hz (azimuthal velocity fluctuations).

smoothed and normalised by their maximum value. The frequency is normalised in the usual manner:

$$\beta = \frac{2\pi r^* f}{U_e}$$

The resulting amplitude spectra are plotted in Figures 9 and 10. All the profiles have a maximum at about the same non-dimensional frequency $\beta \sim 4$ for $x/D > 2$. This behaviour was mentioned previously by Cimbala and Park (1990) who found a peak around $\beta \sim 3$ in the two-dimensional jet-propelled momentumless wake. This indicates that there exists a quasi-periodic radial motion caused by some sort of large turbulent structure near the edge of the wake. It can be understood as the ejection of large eddies at the boundary, leading to the intermittent character of the flow. For the small values of x/D, this maximum amplitude occurs for a slightly lower frequency, as was found by Cimbala and Park (1990). Moreover, unlike jet propulsion, the propeller-driven momentumless wake is characterised by a periodic fluid motion, which adds peaks to the spectra, in the initial development region.

4. The far-wake

After the near-wake, which is strongly marked by spectral peaks and the intermediate region, where turbulence is decreasing and the peaks vanish, a third region appears in Figure 5, with a second change in the slope of the maximum turbulence intensity. In Figure 11, the turbulent kinetic energy profile $\overline{q^2}$ has been scaled by its local maximum value $\overline{q_m^2}$ for several axial positions in this zone. It will be noticed that the form is the same for any axial position, illustrating self-similarity of turbulent kinetic energy for $x/D \geq 17.5$ (Faure and Robert, 1996). This result suggest that there might be a self-similar behaviour of the power spectral density functions, as was found in the

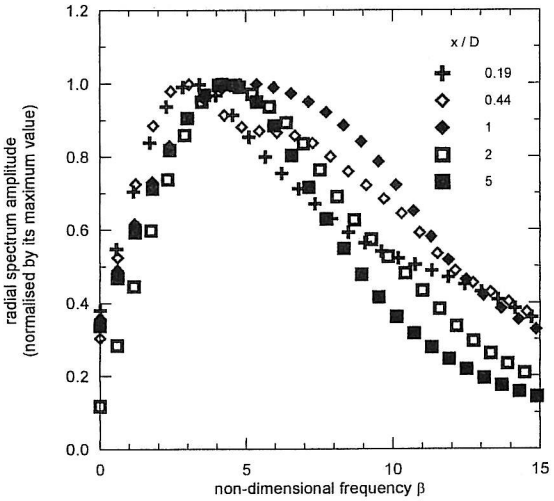

Fig. 9. – Axial evolution of the relative power spectral density function of the radial velocity fluctuations for $x/D \leq 5$.

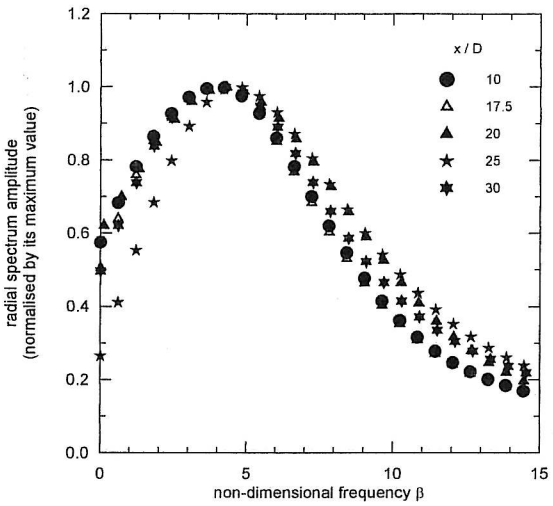

Fig. 10. – Axial evolution of the relative power spectral density function of the radial velocity fluctuations for $x/D \geq 10$.

two-dimensional wake by Wygnanski *et al.* (1986). In Figures 12 and 13 we plot the power spectral density functions of the axial velocity normalised with its zero value, as a function of the non-dimensional frequency β. In Figure 12, the spectra measured on the centreline are plotted for different axial positions in the wake; a self-similar behaviour is found since the discrepancy between the curves is not greater than the measurement error. Furthermore, spectra for an axial location where self-similarity is attained are plotted for different radial positions in Figure 13. The spectra are very close for any radial position inside the wake, leading to an equilibrium between the different

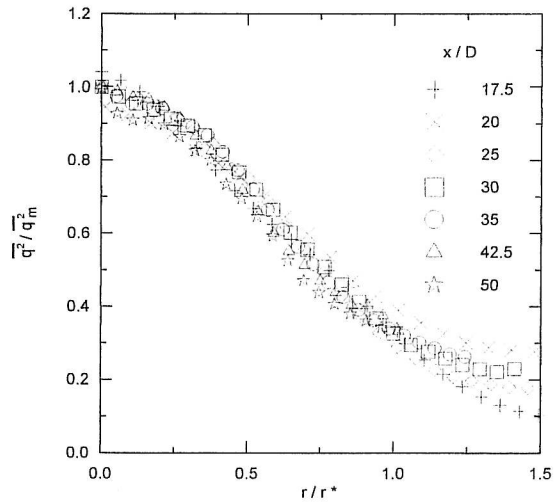

Fig. 11. – Self-similarity of the turbulent kinetic energy profiles in the far wake.

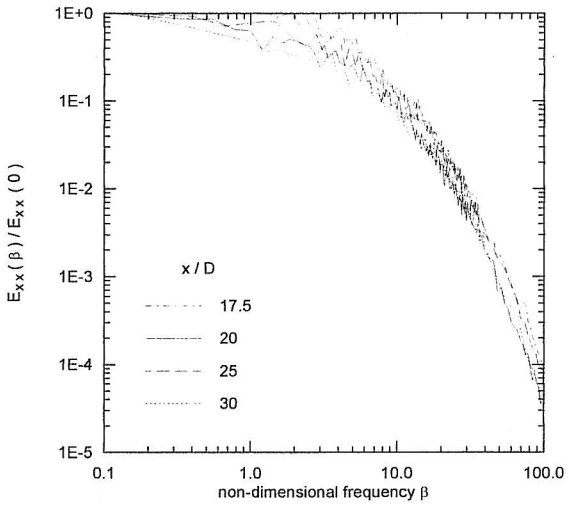

Fig. 12. – Axial evolution for $r/r^* = 0$ of the relative power spectral density function of the axial velocity fluctuations.

turbulent scales. Then, in the far-wake, the turbulent transfer from the large to the small structures is qualitatively the same in the radial and in the axial directions. In addition, the comparison with the spectrum measured in the freestream indicates that this behaviour is not very far from that of grid turbulence. This remark confirms the conclusion of Naudascher (1965) and Cimbala and Park (1990) for jet-propelled momentumless wake. Finally, for a far-momentumless-wake with or without swirl, the bahaviour is relatively close to decaying homogeneous turbulence.

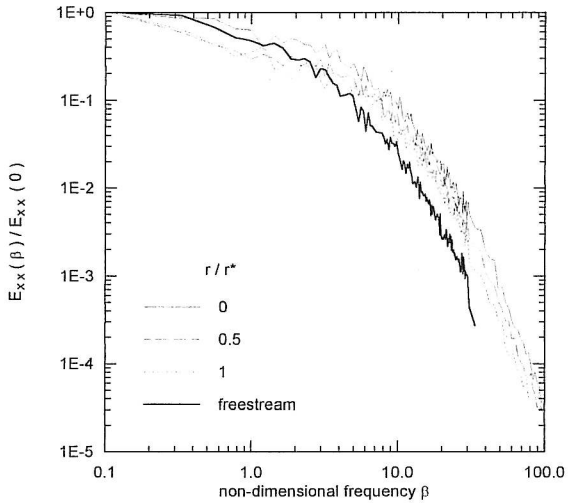

Fig. 13. – Radial evolution for $x/D = 20$ of the relative power spectral density function of the axial velocity fluctuations.

5. Isotropy of turbulence

In this last part, the closeness of the far-wake to decaying homogeneous turbulence is discussed in the context of isotropy. There are few real turbulent flows in which the turbulence can be assumed to be isotropic. However, in high-Reynolds-number flows, the energy is mostly dissipated at the smallest scales of motion which do not receive energy directly from the mean flow, but through an energy transfer from large to small scales. This transfer process removes the directional information of the energy-containing eddies so that the small scales could be considered to be locally isotropic. For such locally isotropic flows, only the statistical properties of the smallest scales of motion would be expected to satisfy the isotropic relations, and there are some implications for the evaluation of the dissipation function. The way to determine this function correctly is to measure all the second-order moments of the derivatives of velocity fluctuations. This was done by Browne *et al.* (1987) who determined with care the nine terms that make up the total dissipation in the self-similar region of a cylinder wake. But this method is difficult and requires special arrangements of multiple miniature X-wire probes. Another approach, used more often, is to determine the function from isotropic turbulence and Taylor's hypothesis; thus, dissipation requires only the measurement of the second-order moment of the time derivatives of the axial velocity fluctuations (Taylor, 1935):

$$\varepsilon = 15\nu\overline{\left(\frac{\partial u_x}{\partial x}\right)^2} \approx \frac{15}{\overline{U}_x^2}\,\nu\overline{\left(\frac{\partial u_x}{\partial t}\right)^2}$$

However, it was shown by Browne *et al.* (1987) that this estimate gives about 20% of the real dissipation on the cylinder wake centreline, where the Reynolds number

based on the Taylor microscale λ, and the root mean squared value of the axial velocity fluctuation, was $\mathrm{Re}_\lambda = 40$. An argument for the appropriate use of the isotropic estimate of dissipation is a large value of Re_λ. In the present investigation, $\mathrm{Re}_\lambda = 140$ on the centreline of the far-wake. However, there is more evidence to suggest how isotropic are the structures which have a significant contribution to the dissipation function. The one-dimensional wavenumber spectrum E_{xx} is scaled by $\varepsilon^{1/4}\nu^{5/4}$, where ν is the kinematic viscosity, and plotted for this location and compared with other experiments in Figure 14. On the abscissa axis the wavenumber k_x multiplied with the Kolmogorov scale η is non-dimensional. This compilation of data is from McComb (1990) and Saddoughi and Veeravalli (1994). We note that the spectrum fits with the other curves, and for the momentumless wake the $-5/3$ Kolmogorov law is validated for $0.03 \leq k_x\eta \leq 0.1$, where the upper limit corresponds to the boundary between inertial and dissipation effects. For greater wavenumbers, in the dissipative region, the experimental spectrum is in good agreement with the universal function. This figure however can not provide a definite indication of how nearly the dissipation corresponds to the isotropic case.

Knowledge of the axial, radial and azimuthal spectral allows a determination of the ratios K_1 and K_2 defined as:

$$K_1 = 2\overline{\left(\frac{\partial u_x}{\partial x}\right)^2} \Big/ \overline{\left(\frac{\partial u_r}{\partial x}\right)^2} \qquad K_2 = 2\overline{\left(\frac{\partial u_x}{\partial x}\right)^2} \Big/ \overline{\left(\frac{\partial u_\theta}{\partial x}\right)^2}$$

Note that the expected value for isotropic turbulence is one; nevertheless, this is never the case in experiments. The radial evolution of these ratios in the far-wake is given in Figure 15. They are both smaller than one; this result is surprising, if you compare it with the compilations given by Browne *et al.* (1987) and completed by George and Hussein (1991), because K_1 and K_2 are generally greater than one. While constant values for K_1 and K_2 cannot be rigorously assumed, the hill and valley behaviour of these two ratios is similar to that obtained by Browne *et al.* (1987). These variations are probably due to the uncertainties involved in evaluating experimental derivatives.

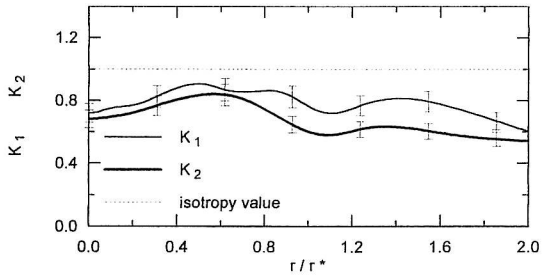

Fig. 15. – Radial evolution of the ratios K_1 and K_2 in the self-similar wake.

6. Concluding remarks

A velocity spectrum investigation was carried out in the turbulent wake of a rotor-driven body, providing new data about this momentumless flow. The near-wake is

strongly marked by spectral peaks related to the propeller rotational frequency f_0 and the blade passing frequency $3f_0$. The latter is dominant at the beginning of the wake but vanishes more rapidly around $x/D \sim 2$, whereas the peak at f_0 remains to $x/D \sim 5$. These peaks contain a large amount of energy which is transferred to the turbulent motion. Another noteworthy result which is valid for any axial position is the wide-band part of the spectrum for the radial velocity fluctuation; it shows a maximum for a radial location corresponding to the edge of the wake. This maximum can be associated with a large scale turbulent motion near the wake boundary and is similar to that found in a jet-propelled momentumless wake. Furthermore, spectra evolve to self-similarity in the far-wake, and are not very far from homogeneous turbulence, as was assumed in previous studies. Finally, the closeness of the flow to decaying homogeneous turbulence suggests

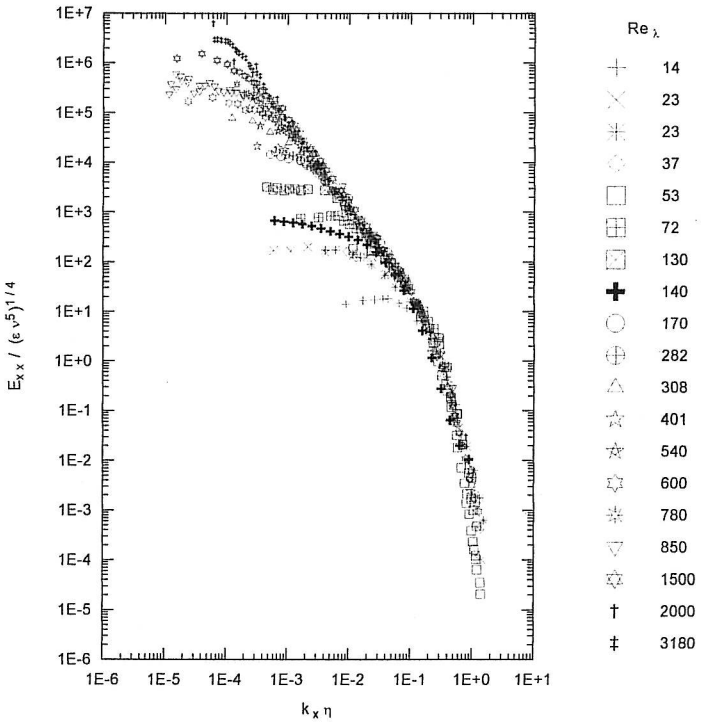

Fig. 14. – Kolmogorov's universal scaling for one-dimensional longitudinal power spectra. This compilation of data is from McComb (1990) and Saddoughi and Veeravalli (1994). The various symbols are associated with different Reynolds numbers referring to the following investigations: 14 grid turbulence (Stewart and Townsend, 1951); 23 wake behind cylinder (Uberoi and Freymuth, 1969); 23 boundary layer (Tielman, 1967); 37 grid turbulence (Comte-Bellot and Corrsin, 1971); 53 channel centreline (DNS Kim and Antonia, 1991); 72 grid turbulence (Comte-Bellot and Corrsin, 1971); 130 homogeneous shear flow (Champagne *et al.*, 1970); 140 momentumless wake (present investigation); 170 pipe flow (Laufer, 1954); 282 boundary layer (Tielman, 1967); 308 wake behind cylinder (Uberoi and Freymuth, 1969); 401 boundary layer (Sandborn and Marshall, 1965); 540 grid turbulence (Kistler and Vrebalovich, 1966); 600 boundary layer (Saddoughi and Veeravalli, 1994); 780 round jet (Gibson, 1963); 850 boundary layer (Coantic and Favre, 1974); 1500 boundary layer (Saddoughi and Veeravalli, 1994); 2000 tidal channel (Grant *et al.*, 1961); 3180 return channel (CAHI Moscow, 1991).

a comparison of the far-momentumless-wake with isotropic turbulence. Measurements of the ratios K_1 and K_2 were carried out.

Acknowledgements

We wish to thank Professor J. N. Gence and Dr L. Le Penven for valuable discussions during the course of this work.

REFERENCES

BENDAT J. S., PIERSOL A. G., 1986, *Random Data: Analysis and Measurement Procedures*, John Wiley & Sons.

BROWNE L. W. B., ANTONIA R. A., SHAH D. A., 1987, Turbulent energy dissipation in a wake, *J. Fluid Mech.*, **179**, 307-326.

CHAMPAGNE F. H., HARRIS V. G., CORRSIN S., 1970, Experiments on nearly homogeneous turbulent shear flow, *J. Fluid Mech.*, **41**, 81-139.

CHIENG C. C., JAKUBOWSKI A. K., SCHETZ J. A., 1974, *Investigation of the Turbulent Properties of the Wade Behind Self-propelled, Axisymmetric Bodies*, Office of Naval Research, VPI-Aero-025.

CIMBALA J. M., KREIN M. V., 1990, Effect of freestream conditions on the far wake of a circular cylinder, *AIAA J.*, **28**, 1369-1373.

CIMBALA J. M., NAGIB H. M., ROSHKO A., 1988, Large structure in the far wakes of two-dimensional bluff bodies, *J. Fluid Mech.*, **190**, 265-298.

CIMBALA J. M., PARK W. J., 1990, An experimental investigation of the turbulent structure in a two-dimensional momentumless wake, *J. Fluid Mech.*, **213**, 479-509.

COANTIC M., FAVRE A., 1974, Activities in, and preliminary results of, air-sea interactions research at I.M.S.T., *Advances in Geophysics*, **18A**, 391-405.

COMTE-BELLOT G., CORRSIN S., 1971, Simple Eulerian time correlation of full and narrow-band velocity signals in grid-generated "isotropic" turbulence, *J. Fluid Mech.*, **48**, 273-337.

FAURE T., 1995, *Étude expérimentale du sillage turbulent d'un corps à symétrie de révolution autopropulsé par hélice*, Ph.D. Thesis, École Centrale de Lyon, n° 95-01.

FAURE T., ROBERT G., 1996, Turbulent kinetic energy balance in the wake of a self-propelled body, *Exp. Fluids*, **21**, 268-274.

GEORGE W. K., HUSSEIN H. J., 1991, Locally axisymmetric turbulence, *J. Fluid Mech.*, **233**, 1-23.

GIBSON M. M., 1963, Spectra of turbulence in a round jet, *J. Fluid Mech.*, **15**, 161-173.

GRANT H. L., STEWART R. W., MOILLIET A., 1961, Turbulence spectra from a tidal channel, *J. Fluid Mech.*, **12**, 241-268.

HIGUCHI H., KUBOTA T., 1990, Axisymmetric wakes behind a slender body including zero-momentum configurations, *Phys. Fluids A*, **2**, 1615-1623.

HYUN B. S., PATEL V. C., 1991, Measurements in the flow around a marine propeller at the stern of an axisymmetric body/Part 1: Circumferentially-averaged flow, *Exp. Fluids*, **11**, 33-44, Part 2: Phase-averaged flow, *Exp. Fluids*, **11**, 105-117.

JONES F. L., RITZ C. P., MIKSAD R. W., POWERS E. J., SOLIS R. S., 1988, Measurement of the local wavenumber and frequency spectrum in a plane wake, *Exp. Fluids*, **6**, 365-372.

KISTLER A. L., VREBALOVICH T., 1966, Grid turbulence at large Reynolds numbers, *J. Fluid Mech.*, **26**, 37-47.

LAUFER J., 1954, *The Structure of Turbulence in Fully Developed Pipe Flow*, NACA Report 1174.

MC COMB W. D., 1990, *The Physics of Fluid Turbulence*, Oxford Science Publications.

NAUDASCHER E., 1965, Flow in the wake of self-propelled bodies and related sources of turbulence, *J. Fluid Mech.*, **22**, 625-656.

PARK W. J., CIMBALA J. M., 1991, The effect of jet injection geometry on two-dimensional momentumless wakes, *J. Fluid Mech.*, **224**, 29-47.

PETERSON L. F., HAMA F. R., 1978, Instability and transition of the axisymmetric wake of a slender body of revolution, *J. Fluid Mech.*, **88**, 71-96.

SADDOUGHI S. S., VEERAVALLI S. V., 1994, Local isotropy in turbulent boundary layers at high Reynolds number, *J. Fluid Mech.*, **268**, 333-372.

SANDBORN V. A., MARSHALL R. D., 1965, *Local Isotropy in Wind Tunnel Turbulence*, Colorado State University Report CER 65 UAS-RDM71.

SCHETZ J. A., JAKUBOWSKI A. K., 1975, Experimental studies of the turbulent wake behind self-propelled slender bodies, *AIAA J.*, **13**, 1568-1575.

SCHOOLEY A. H., STEWART R. W., 1963, Experiments with a self-propelled body submerged in a fluid with a vertical density gradient, *J. Fluid Mech.*, **15**, 83-99.

STEWART R. W., TOWNSEND A. A., 1951, Similarity and self-preservation in isotropic turbulence, *Phil. Trans. Roy. Soc. London* A, **243**, 359-386.

SWANSON Jr. R. C., SCHETZ J. A., JAKUBOWSKI A. K., 1974, *Turbulent Wake Behind Slender Bodies Including Self-Propelled Configurations*, Office of Naval Reseach, VPI-Aero-024.

TAYLOR G. I., 1935, Statistical theory of turbulence, *Proc. Roy. Soc. London* A, **151**, 421-478.

TIELMAN H. W., 1967, *Viscous Region of Turbulent Boundary Layer*, Colorado State University Report CER 67-68 HWT21.

UBEROI M. S., FREYMUTH P., 1969, Spectra of turbulence in wakes behind circular cylinders, *Phys. Fluids* A, **12**, 1359-1363.

WYGNANSKI I., CHAMPAGNE F., MARASLI B., 1986, On the large-scale structures in two-dimensional, small-deficit, turbulent wakes, *J. Fluid Mech.*, **168**, 31-71.

WYNGAARD J. C., PAO Y. H., 1971, Some measurements of the fine structure of large Reynolds number turbulence, *Statistical Models and Turbulence*, edited by M. Rosenblatt and C. Van Atta, Springer-Verlag, Berlin, 384-401.

(Manuscript received February 15, 1996;
revised September 3, 1996;
accepted October 14, 1996.)